Nanoscale Advances

ROYAL SOCIETY OF CHEMISTRY

PAPER

View Article Online
View Journal | View Issue

Cite this: *Nanoscale Adv.*, 2021, **3**, 3177

Flexible core–shell Cs_xWO_3-based films with high UV/NIR filtration efficiency and stability

Yang Wang, Zhendong Yan, Mengfei Zhang, Zheng Zhang, Ting Li, Mingqing Chen and Weifu Dong *

Cesium-doped tungsten bronze Cs_xWO_3 (CWO) is an ideal near infrared (NIR) shielding material for solar filters. However, the NIR shielding ability of CWO-dispersed films easily deteriorates in hot humid environments, which severely hinders the commercial application of CWO. In this paper, UV/NIR shielding nanocomposite films were prepared by dispersing core–shell structured CWO@polydopamine (CWO@PDA) in a poly(vinyl alcohol) matrix. Because of the strong ultraviolet light absorption ability of PDA, it can shield ultraviolet light, which is generally detrimental to our health. The prepared nanocomposite films can efficiently shield 88.3% UV and 85.5% NIR radiation even though they show relatively high transparency in the visible range. Importantly, the good protection of the continuous PDA shells played an important role in enhancing the stability of CWO nanoparticles. The nanocomposite films also exhibit excellent stability in hot humid environments. Therefore, core–shell structured CWO@PDA nanoparticles have great potential as a novel UV/NIR shielding material for the development of efficient energy-saving windows.

Received 11th February 2021
Accepted 26th March 2021

DOI: 10.1039/d1na00113b

rsc.li/nanoscale-advances

Introduction

The global demand for energy increases every year, whereas the amount of useable energy resources, such as fossil fuels, decreases. Thus, developing new energy-saving materials is becoming increasingly important. A large amount of the world's energy is consumed in maintaining indoor comfort of offices and houses *via* air conditioning and heat shielding.[1] Windows play an important role in building lighting and ventilation. In addition, automobiles require high performance heat generating and heat shielding windows for removing ice or frost on the window and blocking sunlight from outside. More than 50% of the total energy is spent on air conditioning and heating, and a significant amount of this energy is lost because of poor thermal shielding and/or insulation of windows.[2,3] However, normal window glasses cannot provide a shield against near-infrared light in the solar energy spectrum, which increases the indoor temperature during summer.[4–8]

It is well known that solar light is chiefly concentrated in the wavelength range between 200 and 2500 nm, including ultraviolet (UV, a wavelength of 200 to 400 nm, 4% of total energy), visible (400–780 mm, 46% of the total energy), and near infrared (NIR, 780–2500 nm, 50% of total energy) light.[9] Therefore, synthesizing a material with high NIR shielding ability, which can be used in thermal insulation materials, is an important method to reduce energy losses.

To date, many particles with transparent thermal insulation properties have been reported, such as lanthanide boride (LaB_6), antimony doped tin oxides (ATO), indium tin oxide (ITO), tungsten suboxide ($W_{18}O_{49}$) and vanadium dioxide *etc.*[9–16] However, there are some drawbacks within these particles which restrict their commercial application in the field of energy-saving materials to some extent. For instance, the raw materials for preparing ITO are expensive, and the cut-off wavelength is higher than 1200 nm, which will lead to a lower NIR shielding rate in the short-wavelength region (780–1200 nm). In addition, the visible transparency of VO_2 is still not ideal for daylighting of rooms. By contrast, tungsten bronzes (M_xWO_3, M = Li, Na, K, Rb, Cs, *etc.*) can selectively cut off near infrared light, while maintaining high visible transmittance.[17–22] In particular, Cs-doped tungsten bronze (Cs_xWO_3, abbreviated as CWO) has been brought into practical application for laminated glasses and solar control films of various architectural and automotive windows. Cs^+ can be inserted into the crystal lattice and form the mixed chemical valence of W^{6+} and W^{5+}, to exhibit strong Localized Surface Plasmon Resonance absorption in the NIR range.[23–25] Wu *et al.* fabricated a smart window by rationally selecting Cs_xWO_3 and thermoresponsive poly(*n*-isopropyl acrylamide) microgels embedded in a polyacrylamide hydrogel matrix as the controllable optical switching material.[5] For example, Yu *et al.* demonstrated a Cs_xWO_3/transparent wood, with a high transmittance in the visible light region and excellent shielding ability of NIR light, for potential energy-saving applications.[26] However, to directly

Key Laboratory of Synthetic and Biological Colloids, Ministry of Education, School of Chemical and Material Engineering, Jiangnan University, 1800 Lihu Road, Wuxi 214122, China. E-mail: wfdong@jiangnan.edu.cn

apply inorganic nanoparticles and polymer composites, some problems related to the reliability of the products must be overcome. First, inorganic nanoparticles always exhibit photocatalytic activity and can photo-degrade organic materials. Second, avoiding the aggregation of nanoparticles in the polymer matrix is often difficult because of the presence of strong interparticle interactions and weak interfacial interactions between nanoparticles and polymers. In particular, M_xWO_3-dispersed films often show slight chromatic instabilities in weathering evaluations, *i.e.*, they enhance a bluish tint when illuminated by strong UV light, while they bleach the bluish tint when subjected to prolonged heating in air, in high humidity, or in water.[27,28] These serious problems about the instabilities of tungsten bronzes in weathering evaluations cast a shadow on the prospect of commercial applications. On the other hand, M_xWO_3 has relatively low absorbance in the UV region. Overexposure to UV radiation may cause damage to human health and material property. For simultaneously satisfying visual effects and reducing the heating/adverse effect, it is necessary to develop UV/NIR-shielding materials which can only transmit visible light but cut off both NIR and UV light.

Polydopamine (PDA) is also a major pigment of naturally occurring melanin (eumelanin). PDA displays many striking properties of naturally occurring melanin in electricity, and magnetics, and, most importantly, it possesses excellent UV light absorption properties.[29,30] The primary advantage of polydopamine is that, as seen with mussels, it can be easily deposited on virtually all types of inorganic and organic substrates, including superhydrophobic surfaces, with a controllable film thickness and durable stability.[31,32] In our previous work, we first coated the surface of copper nanowires (CuNWs) with the PDA layer. The PDA not only protected the CuNW from being oxidized, but also improved the miscibility and dispersibility of the CuNW in the epoxy matrix.[33] Herein, we present a facile CWO@PDA nanocomposite film, which achieves high NIR shielding efficiency, excellent UV-shielding, and good stability. The as-prepared nanocomposite film can shield 88.3% UV and 85.5% NIR light. The interior air temperature of a box shielded with a PVA/CWO@PDA film ($\Delta T = 6.9$ °C) was smaller than that when the box was shielded with pure PVA ($\Delta T = 17.0$ °C). The CWO core serves as the NIR shielding phase with strong NIR light absorption ability while the PDA shell not only works as a UV absorbent but also hinders the diffusion of oxygen and water vapor. Owing to the protection of the PDA shell, the nanocomposite films exhibit strong stability in hot humid environments.

Experimental section

Materials

Tungsten trioxide nanoparticles (99.8%), cesium carbonate (99.9%), and dopamine (98%) were purchased from Aladdin. All the chemicals above were used without further purification. Poly(vinyl alcohol) (PVA-1799) was supplied from Sinopec Sichuan Vinylon Works.

Preparation of CWO nanoparticles

CWO nanoparticles were prepared according to a reported method.[34] Tungsten trioxide and cesium carbonate were used as raw materials without further purification. The two materials with a W to Cs elemental ratio of 1 : 0.33 were dispersed in distilled water and stirred for 0.5 h at room temperature. This mixture was dried overnight in a vacuum at 80 °C. The resulting powder was annealed for 1 h at 600 °C under a H_2/N_2 atmosphere to prepare the CWO powder.

Preparation of CWO@PDA

CWO (0.1 g) and dopamine (0.1 g) were added to 90 mL deionized water by ultrasonication into a uniform

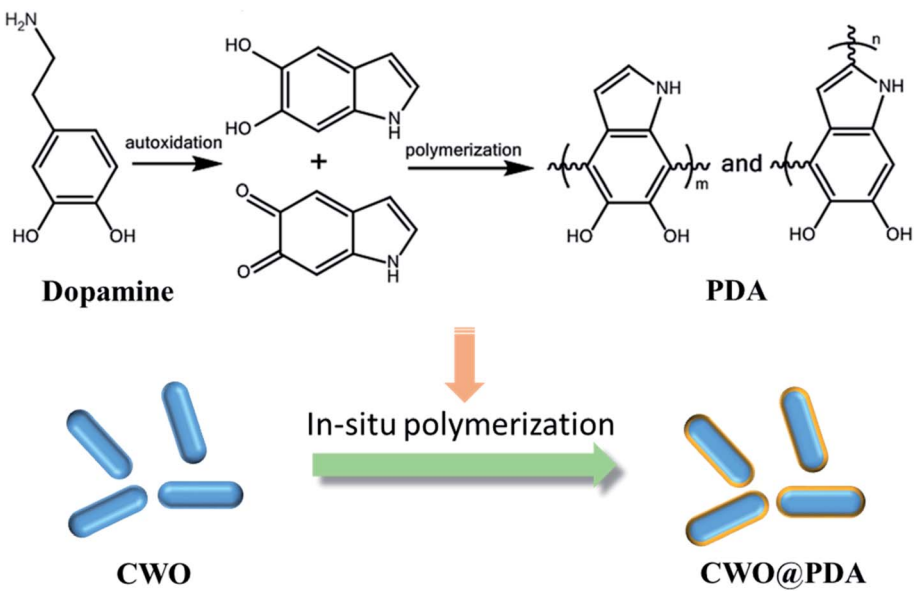

Scheme 1 The synthesis of CWO@PDA nanoparticles.

dispersion. The pH of the mixed solution was adjusted to ~8.5 by adding tris(hydroxymethyl)aminomethane. After that, the suspension was kept at room temperature for 5 h with vigorous stirring. CWO@PDA nanoparticles were collected by centrifugation and then washed with deionized water several times and then dried at 80 °C. The whole process for the synthesis of CWO@PDA nanoparticles is illustrated in Scheme 1.

Preparation of PVA/CWO@PDA nanocomposites

First, PVA solution with a mass concentration of 10 wt% was obtained by dissolving PVA in deionized water with stirring in a 90 °C water bath for 3 h. CWO@PDA powder was dispersed in 15 mL of deionized water by ultrasonication to form a homogeneous suspension. Subsequently, the as-prepared PVA solution was added, and the mixed solution was dispersed well by strong magnetic stirring for 2 h. Finally, the dispersed solution was painted on glass to form composite films using the rolling coating method. The prepared films were dried at room temperature for 12 h and then further dried in an air-circulating oven at 50 °C for 6 h to remove water completely. The resulting films were quite uniform with an average thickness of about 100 μm.

Characterization

X-ray diffraction (XRD) was performed using an X-ray diffractometer (Bruker-D8, Germany). Attenuated Total Reflection (ATR) was measured to record infrared spectra using a Nicolet 6700 FTIR spectrometer. The UV-visible-NIR absorption spectrum was measured using a UV-3600 plus spectrophotometer. Thermal gravimetric analysis (TGA) of the sample was performed on a Meteler-Toledo 1100SF instrument from 20 to 800 °C at a heat rate of 20 °C min^{-1} under a nitrogen atmosphere. The morphologies of nanoparticles were characterized by scanning electron microscopy (SEM S4800) and transmission electron microscopy (TEM JEM-2100Plus, Japan). Heat-insulation performance was investigated by measuring the change in the temperature of an insulating box in real time using an electronic thermometer exposed to 300 W xenon lamp irradiation, and the illumination intensity was adjusted to 0.5 W cm^{-2}.

Based on the measurements of the optical performances of PVA/CWO@PDA nanocomposites, the NIR shielding ability was assessed quantitatively by calculating the solar energy transmittance selectivity (SETS). SETS was obtained through eqn (1):[35]

$$\mathrm{SETS} = \frac{1}{2}\left(1 + \frac{\int_{UV}^{vis} E(\lambda)T(\lambda)\mathrm{d}\lambda}{\int_{UV}^{vis} E(\lambda)\mathrm{d}\lambda} - \frac{\int_{UV}^{NIR} E(\lambda)T(\lambda)\mathrm{d}\lambda}{\int_{UV}^{NIR} E(\lambda)\mathrm{d}\lambda}\right) \quad (1)$$

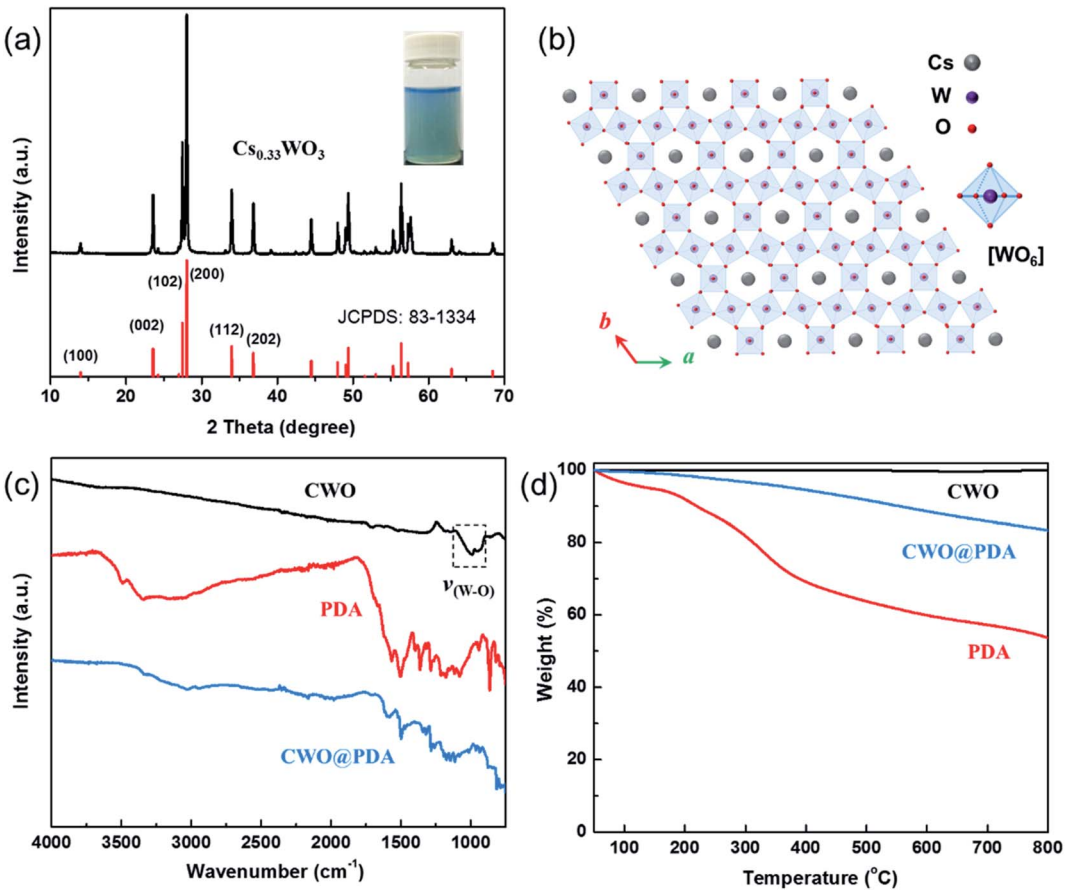

Fig. 1 (a) XRD pattern of CWO with the standard diffraction of $Cs_{0.33}WO_3$ and the (b) structure framework of $Cs_{0.33}WO_3$ projected on the *a* and *b* planes. (c) FTIR spectra and (d) TGA curves of samples.

In this equation, $E(\lambda)$ is the solar irradiance spectrum. $T(\lambda)$ is the transmittance spectrum. SETS represents the solar energy transmittance deviation. The value of SETS ranges from 0 to 1. The minimal value of '0' represents a material with visible or ultraviolet light shielding ability; the middle value of '0.5' represents a coating without any light absorption performance. The higher the SETS value is, the more NIR lights are blocked and simultaneously the more visible lights go through, which means that the material is more suitable for application in NIR blocking films.

To characterize the UV-shielding performance of nanocomposite films, Rhodamine B (RhB) solution (10 mg L^{-1}) protected by the composite film was irradiated under a xenon lamp (with 420 nm cut-off filter); the UV-shielding performance was evaluated according to the degradation of Rhodamine B (RhB) solution.[36]

Results and discussion

Fig. 1a shows the XRD pattern of the CWO particle, as all the diffraction peaks can be indexed to those of the $Cs_{0.33}WO_3$ crystals perfectly (JCPDS no. 83-1334), and no impurity peaks are present. The hexagonal CWO is composed of corner-sharing WO_6 octahedral arrays and Cs atoms located randomly in the one-dimensional hexagonal channels of the WO_6 octahedral framework (Fig. 1b).

To demonstrate the success of this PDA coating process, an FTIR spectrum was used to measure the surface chemistry of CWO@PDA. Fig. 1c shows the FTIR spectra of CWO, PDA, and CWO@PDA. PDA has characteristic bands at 1515, 1605, and 3200–3500 cm^{-1} because of the indole/indoline structures and N–H/O–H bonds.[37] The unmodified CWO exhibits no obvious peaks except for the stretching vibrational bands of $\nu_{(W-O)}$. After PDA coating, the infrared analysis results show that the characteristic groups of PDA exist in the products.

The relative amount of PDA coating was investigated with TGA and is depicted in Fig. 1d. The weight loss of PDA is 46.3% at temperatures up to 800 °C. CWO shows no weight loss. After modification with PDA, a 16.4% weight loss was noted. This indicates that the percentage of PDA of CWO@PDA is 35.4%.

Fig. 2 shows the size and shape of CWO and CWO@PDA nanoparticles. It can be seen that the prepared CWO is nonhomogeneous and the shape is irregular. Fig. 2c shows the TEM image of CWO@PDA. A layer was observed as a light shell and coated on the dark CWO. The encapsulation boundary is clear because the PDA shell is successfully coated on CWO.

The optical properties of the CWO@PDA aqueous dispersion was studied by using UV-vis-NIR spectroscopy (Fig. 3). PDA reveals a well-known, monotonic, and broad-band light absorption. The spectrum of CWO exhibits short-wavelength absorption edged at approximately 600 nm. One can find a relatively low absorbance in the visible region (400–780 nm), indicating that part of the visible region can be transmitted through the CWO solution. Importantly, the spectrum also shows an increased absorption with the increase of wavelength from 700 nm to 1300 nm. The strong NIR photo-absorption is

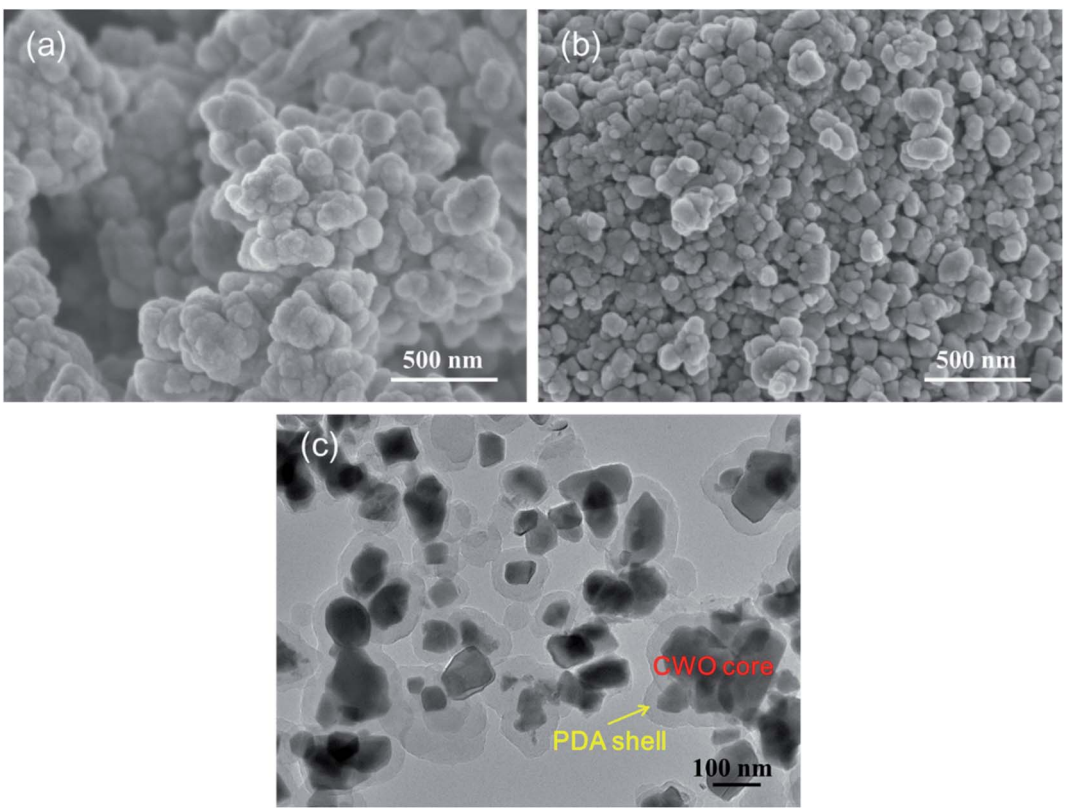

Fig. 2 SEM images of (a) CWO and (b) CWO@PDA. (c) TEM image of core–shell structured CWO@PDA.

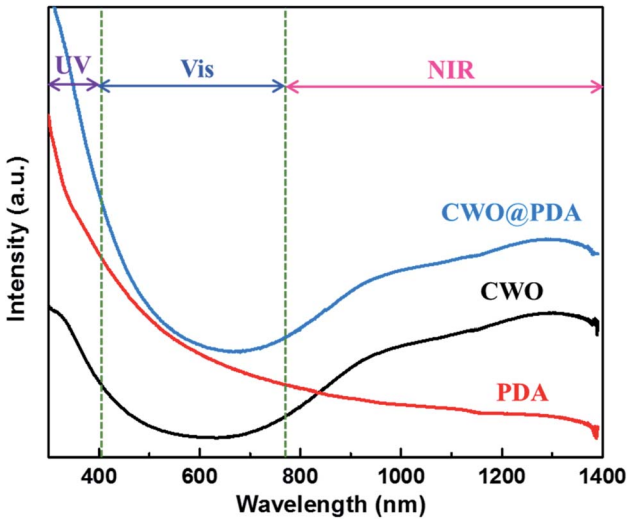

Fig. 3 UV-vis-NIR absorption spectrum of the aqueous dispersion containing PDA, CWO, and CWO@PDA, respectively (30 μg mL^{-1}).

characteristic of CWO nanomaterials, resulting from the strong Localized Surface Plasmon Resonances absorption in the NIR range.[24]

The optical properties of these PVA/CWO@PDA films were studied using a UV-visible-NIR spectrophotometer. For comparison, the transmittance spectrum of pure PVA and PVA/PDA films was also measured. As shown in Fig. 4a, the pure PVA film exhibits high transmittance (≥90%) in the entire UV-vis-NIR region (300–2500 nm), indicating very low photoabsorption in the broad wavelength range. The PVA/PDA film shows relatively high transmittance in the NIR region but low transmittance in the UV region. With the increase of CWO@PDA from 0.2 to 1 wt%, the entire transmittance goes down, where the maximum transmittance at 553 nm drops from 87.2% to 71.9%, and the average transmittance in 1100–2000 nm also decreases from 49.2% to 10.5%. All these results suggest that PVA/CWO@PDA films can transmit part of visible but absorb strongly NIR light. This visible transmittance and NIR shielding behavior of the nanocomposite films should be attributed to the core of CWO@PDA nanoparticles, since the CWO core can absorb efficiently NIR light. On the other hand, the nanoparticles can inevitably lead to light scattering. Furthermore, we also find that the transmittance in the UV region declines with the addition of CWO@PDA, indicating a high UV shielding effect (Fig. 4b). Thus, the UV/NIR shielding performance of the composite film is due to a synergistic relationship between the CWO core and PDA shell.

To compare the NIR shielding performances of these materials quantitatively, some optical indices are listed in Table 1. It can be seen that the SETS (the solar energy transmittance selectivity, eqn (1)) value of the PVA/CWO@PDA (1 wt%) film is 0.729 which is much higher than the SETS value (0.479) of the pure PVA film, indicating that PVA/CWO@PDA nanocomposite films are more suitable as NIR shielding materials.

To characterize the stability of the CWO@PDA nanoparticles in a hot humid environment, the CWO@PDA coatings were kept at 60 °C with 90% humidity in a constant temperature-humidity chamber. Fig. 4c reveals some quantitative results about the

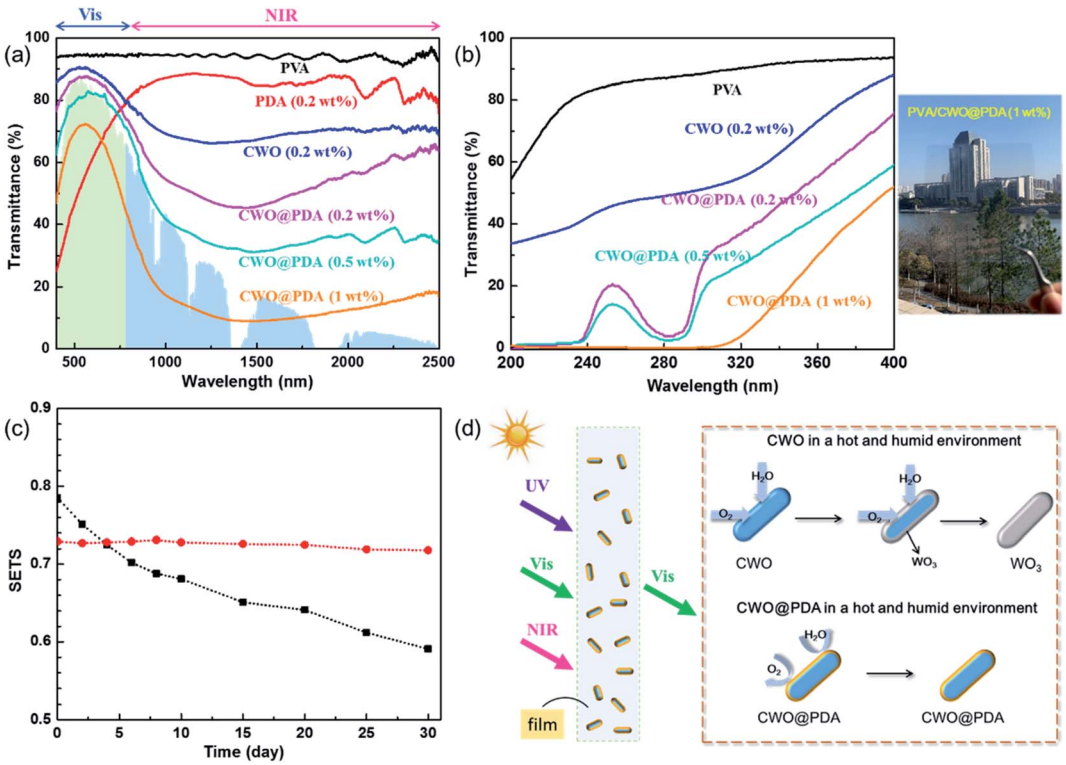

Fig. 4 (a and b) Transmittance spectra of the nanocomposite films (with a thickness of 100 μm). (c) Curves of SETS values *versus* durations. (d) Illustration of the failure mechanisms of CWO and the protective mechanisms of the PDA shells of CWO@PDA.

Table 1 The calculated data of SETS for different (vis and NIR) light of PVA, PVA/PDA, PVA/CWO, and PVA/CWO@PDA nanocomposite films, respectively

Material	Solar energy transmittance of visible lights	Solar energy transmittance of NIR lights	SETS
PVA	0.897	0.939	0.479
PVA/PDA (0.2 wt%)	0.547	0.852	0.348
PVA/CWO (0.2 wt%)	0.829	0.696	0.567
PVA/CWO@PDA (0.2 wt%)	0.792	0.546	0.623
PVA/CWO@PDA (0.5 wt%)	0.738	0.375	0.682
PVA/CWO@PDA (1 wt%)	0.603	0.145	0.729

changes of optical properties in the durability tests. In the extremely harsh environment which was designed to accelerate the possible deterioration behaviors, the SETS value of the PVA/CWO (1 wt%) film degraded evidently from the first day. The curve of the SETS values of the PVA/CWO film dropped from 0.785 to 0.591. The failure mechanism of CWO in a humid environment is illustrated in Fig. 4d. In a humid environment, CWO will be oxidized to WO_3 gradually. During the oxidation process, oxygen plays an essential role and water vapor can accelerate the reaction. The reaction equation can be written as follows (eqn (2)):[38]

$$Cs_{0.33}WO_3 + 0.0825O_2 + 0.165H_2O = WO_3 + 0.33CsOH \quad (2)$$

The attack of oxygen and water vapor takes place on the surface of CWO first. Then oxygen and water vapor will diffuse into the interior of CWO. As a result, more until all the parts of CWO will become WO_3. With the transformation from CWO to WO_3, the selective absorption for NIR light will degrade gradually. Forming core–shell structures can improve the stability of CWO in hot and humid environments. No obvious change was observed in the SETS value of the PVA/CWO@PDA film after even 30 days. Shell materials can hinder the diffusion of oxygen and water vapor, protecting CWO from their attack.

The optical-thermal conversion properties of the obtained nanocomposite films were investigated. The internal temperature changes of the sealed box covered with the nanocomposite films *versus* the irradiation time are illustrated in Fig. 5a. At first, the temperature in the box was ~23.0 °C. After direct exposure for 10 min, the temperature in the box rose to 39.2 °C, 16.2 °C higher than that of the box covered with PVA/CWO@PDA (0.2 wt%). The heating rates of the box covered with the PVA/CWO@PDA films are obviously lower than those of the pure PVA, which indicates that the nanocomposite films have excellent heat insulation properties. After 30 min of irradiation, the temperature equilibrium of all samples was established and remained unchanged with a prolonged irradiation time. The inner temperature of the box covered with the pure PVA reached 40.0 °C, while the boxes covered with PVACWO@PDA (1 wt%) achieved only about 29.9 °C. These results show that PVA/CWO@PDA can be used as a thermal shielding material and has a wide potential application in the field of energy conversation.

In order to confirm the superiority of the PDA layer in improving UV-shielding performance, the UV-shielding performance of PVA nanocomposite films was further examined. RhB solution protected by pure PVA, and PVA/CWO@PDA films was placed under UV light, and the result is shown in Fig. 5b. RhB solution protected by pure PVA presented an obvious degradation, which shows a loss of 76% after UV irradiation for 80 min. However, the light protection efficiency in the UV region increases with the incorporation of CWO@PDA into the PVA matrix. For RhB solution protected by PVA/CWO@PDA (0.2 wt%), about 36.6% of solution degraded. With increasing CWO@PDA concentration to 1 wt%, the degraded content of rhodamine B dropped only 10%, demonstrating an improved UV-shielding efficiency. In general, it is believed that the UV-shielding enhancement is caused by the presence of a PDA layer on the CWO surface, which can help to absorb the UV light and convert the energy of UV light into heat rapidly.

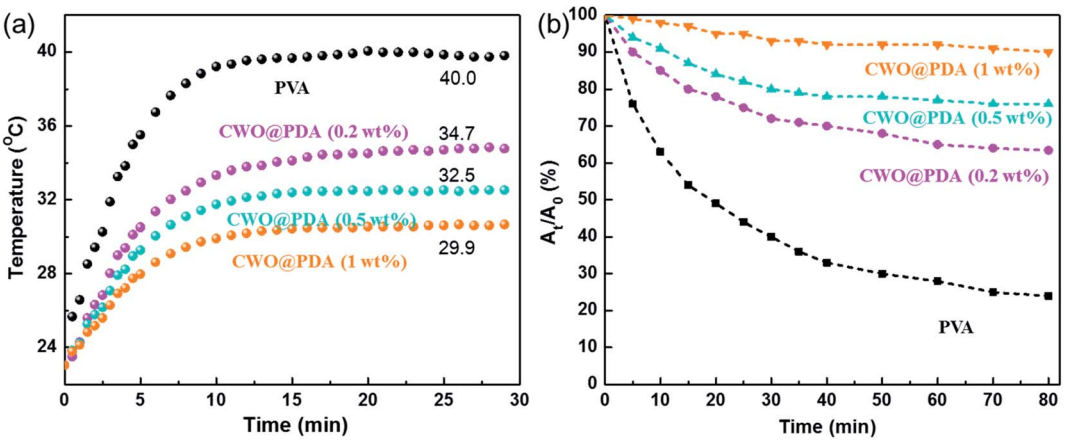

Fig. 5 (a) The curves of the internal temperature with the irradiation time for sealed boxes covered with films. (b) Photodegradation of RhB solution protected by the nanocomposite films.

Conclusions

In summary, core–shell structured CWO@PDA nanoparticles were successfully prepared by a facile method. Polymer nanocomposite films were formed from PVA matrices dispersed with CWO@PDA nanoparticles. The as-prepared films show a strong selective shielding for NIR (85.5%) radiation. Infrared thermal characterization has shown that the proposed nanocomposite film can dramatically reduce the temperature change due to irradiation, providing valid evidence of the CWO@PDA structure's potential as an energy-saving smart material. Meanwhile, these films have a remarkable UV-shielding function (>88.3%) at 200–400 nm for protecting human beings and items from damage and premature aging. More important, the films display excellent stability in hot humid environments.

Conflicts of interest

The authors declare no competing financial interest.

Acknowledgements

This work was supported by the National Natural Science Foundation of China (22005122), the Natural Science Foundation of Jiangsu Province (BK20190612), MOE & SAFEA, and 111 Project (B13025).

References

1 R. Baetens, B. R. P. Jelle and A. Gustavsen, *Sol. Energy Mater. Sol. Cells*, 2010, **94**, 87–105.
2 J. Peng, D. C. Curcija, L. Lu, S. E. Selkowitz, H. Yang and W. Zhang, *Appl. Energy*, 2016, **165**, 345–356.
3 C. Nakamura, K. Manabe, M. Tenjimbayashi, Y. Tokura, K.-H. Kyung and S. Shiratori, *ACS Appl. Mater. Interfaces*, 2018, **10**, 22731–22738.
4 K. Li, S. Meng, S. Xia, X. Ren and G. Gao, *ACS Appl. Mater. Interfaces*, 2020, **12**, 42193–42201.
5 M. Wu, Y. Shi, R. Li and P. Wang, *ACS Appl. Mater. Interfaces*, 2018, **10**, 39819–39827.
6 X. Q. Wang, C. F. Tan, K. H. Chan, K. Xu, M. Hong, S. W. Kim and G. W. Ho, *ACS Nano*, 2017, **11**, 10568–10574.
7 N. Hano, M. Takafuji, H. Noguchi and H. Ihara, *ACS Appl. Nano Mater.*, 2019, **2**, 3597–3605.
8 H. Yuan, T. Li, Y. Wang, P. Ma, M. Du, T. Liu, Y. Yan, H. Bai, M. Chen and W. Dong, *Compos. Commun.*, 2020, **22**, 100443.
9 L. Peng, W. Chen, B. Su, A. Yu and X. Jiang, *Appl. Surf. Sci.*, 2019, **475**, 325–333.
10 T. Chang, X. Cao, N. Li, S. Long, X. Gao, L. R. Dedon, G. Sun, H. Luo and P. Jin, *ACS Appl. Mater. Interfaces*, 2017, **9**, 26029–26037.
11 C. Ding, A. Han, M. Ye, Y. Zhang, L. Yao and J. Yang, *RSC Adv.*, 2018, **8**, 19690–19700.
12 H. Matsui, T. Hasebe, N. Hasuike and H. Tabata, *ACS Appl. Nano Mater.*, 2018, **1**, 1853–1862.
13 P. Jeevanandam, R. S. Mulukutla, M. Phillips, S. Chaudhuri, L. E. Erickson and K. J. Klabunde, *J. Phys. Chem. C*, 2007, **111**, 1912–1918.
14 Y. Bao, R. Guo and J. Ma, *ACS Appl. Mater. Interfaces*, 2020, **12**, 24250–24261.
15 S. K. Kang, D. H. Ho, C. H. Lee, H. S. Lim and J. H. Cho, *ACS Appl. Mater. Interfaces*, 2020, **12**, 33838–33845.
16 H. Y. Lee, Y. Cai, S. Bi, Y. N. Liang, Y. Song and X. M. Hu, *ACS Appl. Mater. Interfaces*, 2017, **9**, 6054–6063.
17 C. Guo, S. Yin, L. Huang and T. Sato, *ACS Appl. Mater. Interfaces*, 2011, **3**, 2794–2799.
18 K. Katagiri, R. Takabatake and K. Inumaru, *ACS Appl. Mater. Interfaces*, 2013, **5**, 10240–10245.
19 S. Zhang, Y. Yang, L. Xu, H. Yu, D. Li, X. Wang and X. Dong, *New J. Chem.*, 2020, **44**, 10418–10427.
20 C. Y. Fan, J. X. Liu, F. Shi, S. Ran, B. Chen, J. Zhou, S.-H. Liu, X. Song and J. Kang, *RSC Adv.*, 2019, **9**, 5804–5814.
21 C. Yang, J. F. Chen, X. Zeng, D. Cheng and D. Cao, *Ind. Eng. Chem. Res.*, 2014, **53**, 17981–17988.
22 Y. Li, J. Liu, J. Liang, X. Yu and D. Li, *ACS Appl. Mater. Interfaces*, 2015, **7**, 6574–6583.
23 W. Chen, T. K. N. Nguyen, M. Wilmet, N. Dumait, O. Makrygenni, Y. Matsui, T. Takei, S. Cordier, N. Ohashi, T. Uchikoshi and F. Grasset, *Nanoscale Adv.*, 2019, **1**, 3693–3698.
24 J. Yang, J. Liu, Y. Qiao, F. Shi, S. Ran, Y. Dong and S. Liu, *CrystEngComm*, 2020, **22**, 573–586.
25 S. Qi, X. Xiao, Y. Lu, C. Huan, Y. Zhan, H. Liu and G. Xu, *CrystEngComm*, 2019, **21**, 3264–3272.
26 Z. Yu, Y. Yao, J. Yao, L. Zhang, Z. Chen, Y. Gao and H. Luo, *J. Mater. Chem. A*, 2017, **5**, 6019–6024.
27 K. Adachi, Y. Ota, H. Tanaka, M. Okada, N. Oshimura and A. Tofuku, *J. Appl. Phys.*, 2013, **114**, 194304.
28 W. H. Lee, H. Hwang, K. Moon, K. Shin, J. H. Han, S. H. Um, J. Park and J. H. Cho, *Fibers Polym.*, 2013, **14**, 2077–2082.
29 Y. Wang, J. Su, T. Li, P. Ma, H. Bai, Y. Xie, M. Chen and W. Dong, *ACS Appl. Mater. Interfaces*, 2017, **9**, 36281–36289.
30 Y. Wang, X. Wang, T. Li, P. Ma, S. Zhang, M. Du, W. Dong, Y. Xie and M. Chen, *ACS Appl. Mater. Interfaces*, 2018, **10**, 13100–13106.
31 Y. Wang, H. Yuan, P. Ma, H. Bai, M. Chen, W. Dong, Y. Xie and Y. S. Deshmukh, *ACS Appl. Mater. Interfaces*, 2017, **9**, 4215–4222.
32 Y. Wang, T. Li, P. Ma, S. Zhang, H. Zhang, M. Du, Y. Xie, M. Chen, W. Dong and W. Ming, *ACS Nano*, 2018, **12**, 6228–6235.
33 H. Yuan, Y. Wang, T. Li, P. Ma, S. Zhang, M. Du, M. Chen, W. Dong and W. Ming, *Compos. Sci. Technol.*, 2018, **164**, 153–159.
34 Y. Zhou, N. Li, Y. Xin, X. Cao, S. Ji and P. Jin, *J. Mater. Chem. C*, 2017, **5**, 6251–6258.
35 X. Zeng, Y. Zhou, S. Ji, H. Luo, H. Yao, X. Huang and P. Jin, *J. Mater. Chem. C*, 2015, **3**, 8050–8060.
36 Y. Wang, T. Li, P. Ma, H. Bai, Y. Xie, M. Chen and W. Dong, *ACS Sustainable Chem. Eng.*, 2016, **4**, 2252–2258.
37 X. Yu, H. Fan, Y. Liu, Z. Shi and Z. Jin, *Langmuir*, 2014, **30**, 5497–5505.
38 Y. Chen, X. Zeng, Y. Zhou, R. Li, H. Yao, X. Cao and P. Jin, *Ceram. Int.*, 2018, **44**, 2738–2744.